

## Observation of Laser-Induced Continuum Structure in Ionization of Sodium

Y. L. Shao,<sup>(1)</sup> D. Charalambidis,<sup>(1)</sup> C. Fotakis,<sup>(1)</sup> Jian Zhang,<sup>(2)</sup> and P. Lambropoulos<sup>(1),(2)</sup>

<sup>(1)</sup>Foundation for Research and Technology, Hellas, Institute of Electronic Structure and Laser,  
P.O. Box 1527, Heraklion 71110, Crete, Greece

and Department of Physics, University of Crete, Crete, Greece

<sup>(2)</sup>Department of Physics, University of Southern California, Los Angeles, California 90089-0484

(Received 3 September 1991)

We report the first observation of an asymmetric autoionizinglike line shape in the ionization of atomic Na due to laser-induced continuum structure. The results are in very good agreement with a theoretical time-dependent analysis employing independently calculated atomic parameters combined with the instrumental parameters of the experiment.

PACS numbers: 32.80.Wr

The purpose of this paper is to report the demonstration of an asymmetric line shape in ionization due to laser-induced continuum structure (LICS). In spite of the vast theoretical literature [1,2] on LICS since the time it was first proposed by Heller and Popov [3], the effect has only been observed in the rotation of polarization [4] of a probe beam and in third-harmonic generation [5,6]. Feldmann *et al.* [7] have reported symmetric peaks in ionization which they correctly recognized as due to the dominance of Raman processes without a pole in the continuum, as confirmed later quantitatively by Dai and Lambropoulos [8]. The only other experimental data showing structure with some asymmetry in ionization have been reported by Hutchinson and Ness [9]. The origin of that structure remains, however, uncertain since it is qualitatively different from the theoretical prediction of Tang, L'Huillier, and Lambropoulos [10]. Although LICS in any of the above three contexts (polarization rotation, harmonic generation, and ionization) is the manifestation of the same coherent interaction within the one-electron continuum, its detection in each context poses special difficulties due to complications from other processes that may mask the structure. Ionization turns out to be more susceptible to such side effects (as demonstrated in this paper), polarization rotation being the most immune, with harmonic generation [11] somewhere in between but closer to ionization.

The process studied in this paper is depicted in Fig. 1 and represents the simplest and most fundamental scheme for the observation of LICS, but yet has resisted detection for fifteen years. Later on, we mention the main reason for this difficulty. The basic observation consists of measuring ionization as a function of  $\omega_a$  with  $\omega_b$  fixed, and the other way around, in the range of frequencies that satisfy the resonance condition  $E_1 + \hbar\omega_a \approx E_2 + \hbar\omega_b$ . Examining the behavior of the structure as a function of the laser intensities and proving that it can be observed at and move with different values of  $\omega_b$  constitute essential elements of confirmation of the origin of the effect. Agreement with a theoretical prediction with *ab initio* atomic parameters constitutes an additional necessary element.

The experimental setup consists of a time-of-flight (TOF) mass spectrometer, in which the Na atoms are in-

troducted in the form of an effusive beam. The beams of the two tunable dye lasers ( $0.2 \text{ cm}^{-1}$  bandwidth, 13 nsec pulse duration, the frequency of one of which is doubled via a barium borate crystal) are combined in a dichroic mirror and cross the atomic beam, focused with a 12-cm  $F$  achromatic lens. The ionized species are extracted with a dc electric field at right angles with respect to the atomic and laser beams through a 2-mm-diam aperture in front of which the two laser beams are focused, so that only ions produced at the focus could reach the micro-channel plate detector. This geometry prevents blending of the laser-induced structure in the ionization spectra with the background ionization which would come from the collection of ions from an extended volume around the focus. In that extended volume, the intensity of the

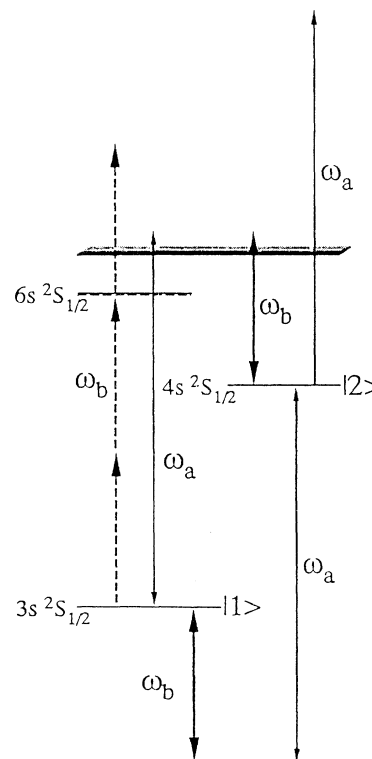


FIG. 1. The most dominant Na energy levels and processes involved in the present study.

TABLE I. Coupling parameters and photoionization widths.  $I_a$  and  $I_b$  are in units of  $\text{W}/\text{cm}^2$ .

$M_{21}\epsilon_a^*\epsilon_b^*$ ( $\text{sec}^{-1}$ )	$q$	$\gamma_1(\omega_a)$ ( $\text{sec}^{-1}$ )	$\gamma_1(3\omega_b)$ ( $\text{sec}^{-1}$ )	$\gamma_2(\omega_a)$ ( $\text{sec}^{-1}$ )	$\gamma_2(\omega_b)$ ( $\text{sec}^{-1}$ )
$1.23(I_a I_b)^{1/2}$	13.3	$0.0449I_a$	$9.58 \times 10^{-25}I_b^3$	$0.0485I_a$	$0.758I_b$

coupling laser  $b$  drops to values not able to produce any detectable structure, but the intensity of laser  $a$  is sufficient for producing significant single-photon ionization which can mask the effect of LICS.

For a rigorous calculation of the expected behavior, one must consider the complete temporal evolution of the atomic system, using accurate atomic parameters and including the appropriate pulse shape employed in the experiment. An additional laser bandwidth needs to be incorporated if the pulse is not Fourier limited and its bandwidth is dominated by stochastic fluctuations [12], as is the case here. With the labeling of Fig. 1 for the states and the photon frequencies, the equations of motion for the slowly varying density matrix describing the time development of the atom under the two fields can be written as

$$\frac{\partial}{\partial t}\sigma_{11} = -[\gamma_1(\omega_a) + \gamma_1(3\omega_b)]\sigma_{11} - 2\text{Im}[\sigma_{12}M_{21}(1+i/q)\epsilon_a^*\epsilon_b], \quad (1)$$

$$\frac{\partial}{\partial t}\sigma_{22} = -[\gamma_2(\omega_a) + \gamma_2(\omega_b)]\sigma_{22} + 2\text{Im}[\sigma_{12}M_{21}(1-i/q)\epsilon_a^*\epsilon_b], \quad (2)$$

$$\left[\frac{\partial}{\partial t} + i\Delta + \Gamma_{12}\right]\sigma_{12} = -iM_{12}\epsilon_a\epsilon_b^*[(1-i/q)\sigma_{22} - (1+i/q)\sigma_{11}], \quad (3)$$

where  $\gamma_1(\omega_a) = \pi|\mu_{1c}(\omega_c = \omega_1 + \omega_a)|^2|\epsilon_a|^2$  is the photoionization width of state 1 by  $\omega_a$ ;  $\gamma_1(3\omega_b) = \pi|\mu_{1c}^{(3)}(\omega_c = \omega_1 + 3\omega_b)|^2|\epsilon_b|^6$  is the three-photon ionization width of state 1 by  $\omega_b$ ;  $\gamma_2(\omega_a) = \pi|\mu_{2c}(\omega_c = \omega_2 + \omega_a)|^2|\epsilon_a|^2$  is the photoionization width of state 2 by  $\omega_a$ ;  $\gamma_2(\omega_b) = \pi|\mu_{2c}(\omega_c = \omega_2 + \omega_b)|^2|\epsilon_b|^2$  is the photoionization width of state 2 by  $\omega_b$ ;  $\Gamma_{12}$  is half of the sum of the four photoionization widths listed above plus the other widths from other broadening mechanisms, in this case the laser bandwidth [12], i.e.,

$$\Gamma_{12} = \frac{1}{2}[\gamma_1(\omega_a) + \gamma_1(3\omega_b) + \gamma_2(\omega_a) + \gamma_2(\omega_b)] + (\omega_a + \omega_b)\beta^2/(\beta^2 + \Delta^2),$$

with the laser bandwidths  $\omega_a = \omega_b = 0.2 \text{ cm}^{-1}$  and  $\beta = 0.5 \text{ cm}^{-1}$  a cutoff parameter such as to prevent unphysical excitation of states far from resonance due to the wing of the Lorentzian;

$$M_{21} = \sum_l \frac{\mu_{2l}\mu_{l1}}{\omega_1 - \omega_l - \omega_b} + P \int d\omega_c \frac{\mu_{2c}\mu_{c1}}{\omega_1 - \omega_l + \omega_a}$$

is the two-photon transition moment between states 1 and 2;  $q = M_{21}/\mu_{2c}\mu_{c1}(\omega_c = \omega_1 + \omega_a)$  is an atomic parameter representing the asymmetry of the absorption peak for either  $\omega_a$  or  $\omega_b$ ;  $\Delta = \omega_a - \omega_b + \omega_1 - \omega_2 + S_1 - S_2$  is the detuning of either laser from the induced resonance in the continuum including the ac Stark shifts of states 1 and 2;  $\epsilon_a$  and  $\epsilon_b$  are the electric-field amplitudes of the two lasers; and  $\mu_{ij} = \langle i | -e\mathbf{r} \cdot \boldsymbol{\epsilon} | j \rangle$  is the electric dipole transition moment between states  $i$  and  $j$  with  $e$  representing the electron charge (negative).

The probability of ionization is given by  $P_{\text{ion}} = 1 - \sigma_{11}(T_L) - \sigma_{22}(T_L)$  where the values of  $\sigma_{11}$  and  $\sigma_{22}$  at the end of the pulse [obtained through the solution of

Eqs. (1)–(3)] must be entered. Under the appropriate conditions, a single-rate equation may describe the line shape well, but usually this can only be justified *a posteriori* [8].

To obtain the atomic dipole transition moments, we have first employed quantum defect theory (QDT). However, due to the fact that the UV laser ionizes the atom only around  $2000 \text{ cm}^{-1}$  above the threshold, QDT may not provide sufficiently accurate numbers. To insure that our matrix elements did not involve errors of more than 10% we also performed independent frozen-core Hartree-Fock calculations. The atomic parameters used in our density-matrix calculations are listed in Table I.

A summary of the main experimental results is shown in Figs. 2 and 3. Figures 2(a)–2(c) show a lower-resolution scan of the wavelength  $\lambda_a$  between 548.5 and 550.0 nm, with  $\lambda_b$  fixed at 227.52 nm, 227.57 nm, and without the coupling laser, correspondingly. The peak at 549.8 nm corresponds to the two-photon resonant three-photon ionization of Na through the  $6s(^2S_{1/2})$  state. The second lower-intensity peak appears only when both laser beams are introduced and its position changes according to the relation  $\hbar\omega_b - \hbar\omega_a = E_2 - E_1$  when the wavelength  $\lambda_a$  is changed. Thus it is verified that this peak is a laser-induced structure. From Fig. 2(c) it can also be verified that the nonresonant three-photon ionization from the ground state due to the coupling laser beam is negligibly small. In Fig. 2(d),  $\lambda_b$  is fixed at 549.2 nm and  $\lambda_a$  is scanned between 227.5 and 227.6 nm. The experimental points are mean values of several experimental runs and the quoted error is 1 standard deviation of the mean value. Since the intensity of the UV radiation generated via frequency doubling showed strong variations

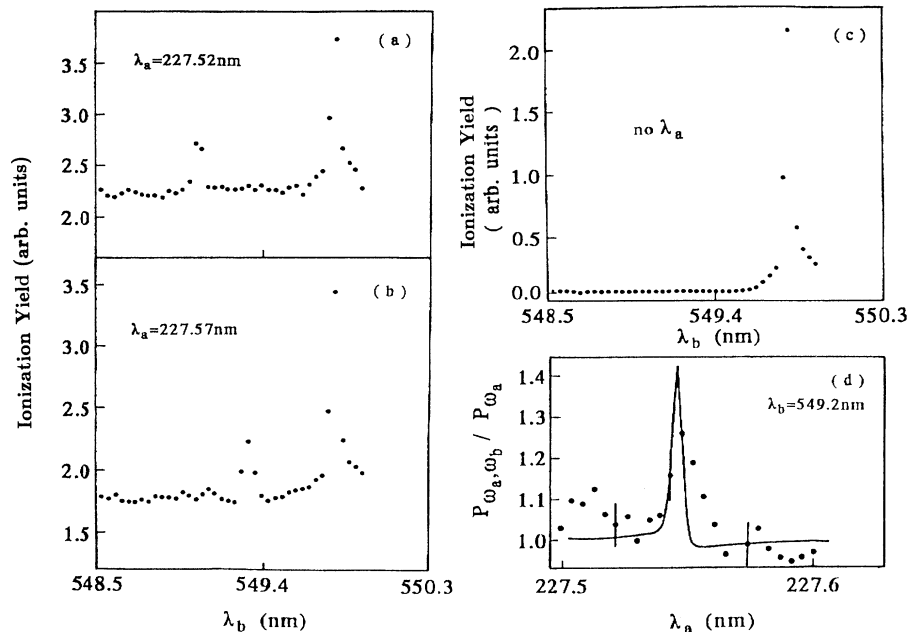


FIG. 2. Ionization spectra of Na scanning  $\lambda_b$  in the region 548.5–550.0 nm and  $\lambda_a$  fixed (a) at 227.52 nm, (b) at 227.57 nm, and (c) without  $\lambda_a$ , and (d) with  $\lambda_b$  fixed at 549.2 nm and  $\lambda_a$  scanned from 227.5 to 227.6 nm. In the last spectrum (d), the ionization yield has been normalized with respect to the ionization yield taken only with  $\lambda_a$ ; the solid curve is the calculated spectrum including ac Stark shifts. The peak at 549.8 nm in (a)–(c) corresponds to the two-photon resonant three-photon ionization of Na through the  $6s(^2S_{1/2})$  state caused by  $\lambda_b$  alone. All other peaks are laser-induced structures due to  $\lambda_b$ .  $I_a \approx 3 \times 10^8$  W/cm<sup>2</sup>,  $I_b \approx 10^9$  W/cm<sup>2</sup>.

with wavelength, the data in Fig. 2(d) have been normalized by the data taken in the absence of the coupling laser beam and the UV laser scanned in the same wavelength region. The variation of the UV output and the normalization procedure account for the larger error bars in Fig. 2(d).

The small asymmetry in the observed laser-induced structure (Figs. 2 and 3) gives strong evidence that the Raman-type processes, i.e., the two-photon coupling of the two bound states, which contribute to the real part of the effective two-photon Rabi frequency, are not dominating in the scheme under investigation due in part to the absence of real states lying near the virtual state of the Raman-type process, unlike the scheme of the earlier work of Feldmann *et al.* [7] where such real near-resonant intermediate states played a dominant role. It is equally important to note that the imaginary part of the effective two-photon Rabi frequency, which comes from the pole of the coupling of the two states through the continuum, is comparable to the real part; which is an essential condition in producing an asymmetric line shape. The resulting dimensionless  $q$  parameter defined earlier provides a qualitative measure of the expected asymmetry. As an indication of the asymmetry inherent in the data at the lower intensities, we note that a  $\chi^2$  fit to the data of Fig. 3(c) using the formula  $(q + \epsilon)^2 / (1 + \epsilon^2)$  yields the value  $q = 16$  while that for the data of Fig. 2(d) yields the value  $q = -3$ .

A power-density dependence of the observed structure in Fig. 2(a) at higher resolution is shown in Fig. 3. The

solid lines are the results of the calculations to which the experimental data have been normalized, since the measurement of the ionization yield is not an absolute one. Besides the “shoulder” on the short-wavelength side of the structure observed at higher power densities, to which we will return at the end of the paper, the agreement between the experiment and the theoretical calculation concerning the dynamic range, the width, and the asymmetry of the structure is very good. Both experiment and theory show, as they should, a reduction of the width of the observed structure as the intensity of  $\omega_b$  is decreased from 15 to 6 GW/cm<sup>2</sup>. This is expected due to the corresponding decrease of the dominant coupling of the  $4s$  to the continuum. The small discrepancy in the height of the peak in Fig. 3(c) can be attributed to the less accurate knowledge of the power density of  $\omega_a$ . Reduction of the intensity of  $\omega_b$  to values smaller than those shown in Fig. 3 makes the observed structure less pronounced and ultimately not detectable, as expected.

In summary, we have demonstrated the existence of asymmetric LICS structure in the smooth continuum of a one-electron atom. The observations are in very good agreement with theory and satisfy all necessary criteria. The most critical step in our experimental technique was the confinement of the observation near the center of the interaction volume combined with mass analysis of the ion. Without this refinement, the signal would have been smeared out by ions from the rest of the interaction volume where the combination of intensities is not appropriate for the creation of LICS. Even with these tech-

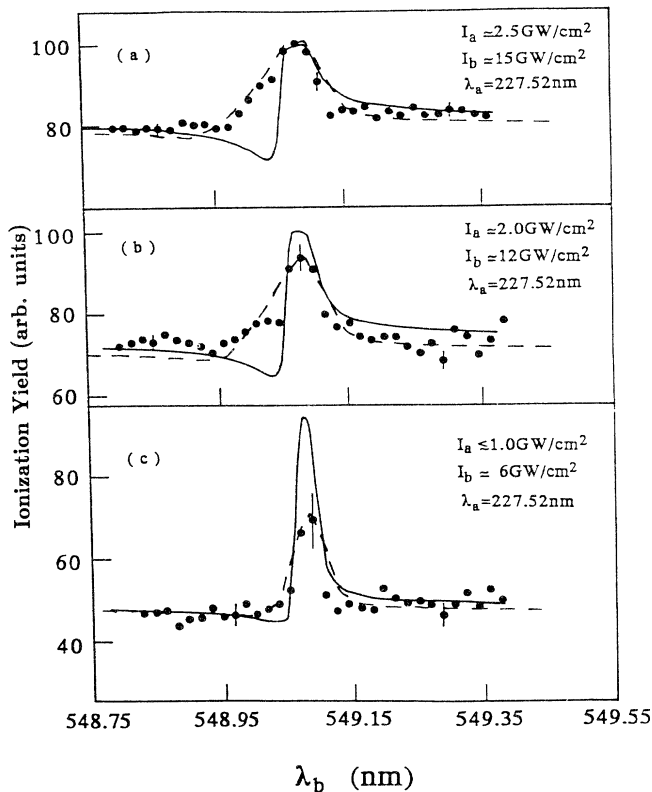


FIG. 3. High-resolution ionization spectra showing the laser-induced structure of Fig. 2(a) at various combinations of laser intensities  $I_a$  and  $I_b$ . The results of the calculation are depicted by solid lines. The points are normalized experimental data. The dashed curves in (a)–(c) are the calculated spectra with ac Stark shifts and volume integration, which become significant at higher intensities.

niques in place, the structure will tend to be smeared for larger values of the intensity  $I_b$  (as saturation begins playing some role even within the limited volume of observation) as well as by ac Stark shifts (due mainly to the stronger field at  $\lambda_b$ ) which are known to lead to asymmetric line broadening in a pulsed field. The shoulders in Figs. 3(a) and 3(b) represent the gradual manifestation of these effects [which play a role even in Fig. 3(c), although not in the form of a shoulder] as confirmed by our calculation that includes the Stark shift and spatial integration—shown by the dashed lines in Figs. 3(a)–3(c). A similar calculation (including the ac Stark shift) also produces very good agreement with the data of Fig. 2(d), where the UV laser has been scanned. Space limitations do not permit further elaboration on the role

of Stark shifts in the line shapes. A detailed theory of the effect of such side effects on LICS has been presented in Ref. [11]. In closing, we should point out that the techniques of this work can be readily employed in the study of harmonic generation in the presence of LICS.

After completion of this work we were informed by Cavalieri, Pavone, and Matera [13] that they have also succeeded in observing similar structure in ionization using the states  $3s$  and  $5s$  of Na in a heat pipe which represents a substantially different environment.

The experiments of the present work have been carried out in the “Ultraviolet Laser Facility” Project No. G/89100086/GEP at FORTH. The theoretical work has been supported by the National Science Foundation under Grant No. PHY-9013434 and by the Department of Energy under Grant No. DE-FG03-87ER60504. Two of us (J.Z. and P.L.) gratefully acknowledge insightful discussions with Xian Tang and communications with S. Cavalieri and M. Matera.

- 
- [1] P. E. Coleman, P. L. Knight, and K. Burnett, *Opt. Commun.* **42**, 171 (1982).
  - [2] P. L. Knight, M. A. Lauder, and B. J. Dalton, *Phys. Rep.* **190**, 1 (1990).
  - [3] Yu. I. Heller and A. K. Popov, *Kvantovaya Elektron. (Moscow)* **3**, 1129 (1976) [*Sov. J. Quantum Electron.* **6**, 606 (1976)].
  - [4] Yu. I. Heller, V. F. Lukinykh, A. K. Popov, and V. V. Slabko, *Phys. Lett.* **82A**, 4 (1981). The same experiment has been successfully repeated recently by S. Cavalieri (private communication).
  - [5] L. I. Pavlov, S. S. Dimov, D. I. Metchkov, G. M. Mileva, and K. V. Stamenov, *Phys. Lett.* **89A**, 441 (1982).
  - [6] S. S. Dimov, L. I. Pavlov, and K. V. Stamenov, *Appl. Phys. B* **30**, 35 (1983).
  - [7] D. Feldmann, G. Otto, D. Petring, and K. H. Welge, *J. Phys. B* **19**, 269 (1986).
  - [8] Bo-nian Dai and P. Lambropoulos, *Phys. Rev. A* **36**, 5205 (1987); **39**, 3704 (1989).
  - [9] M. H. R. Hutchinson and K. M. M. Ness, *Phys. Rev. Lett.* **60**, 105 (1988).
  - [10] X. Tang, A. L’Huillier, and P. Lambropoulos, *Phys. Rev. Lett.* **62**, 111 (1989).
  - [11] J. Zhang and P. Lambropoulos, *Phys. Rev. A* (to be published).
  - [12] P. Zoller and P. Lambropoulos, *J. Phys. B* **12**, L547 (1979).
  - [13] S. Cavalieri, F. S. Pavone, and M. Matera, following Letter, *Phys. Rev. Lett.* **67**, 3673 (1991).